Asymmetry of tensile versus compressive elasticity and permeability contributes to the regulation of exchanges in collagen gels

Jean Cacheux, Jose Ordonez-Miranda, Aurélien Bancaud, Laurent Jalabert, Daniel Alcaide, Masahiro Nomura, Yukiko Matsunaga

APPLIED SCIENCES AND ENGINEERING

Asymmetry of tensile versus compressive elasticity and permeability contributes to the regulation of exchanges in collagen gels

Jean Cacheux[1,2], Jose Ordonez-Miranda[1,2], Aurélien Bancaud[1,2,3]*, Laurent Jalabert[1,2], Daniel Alcaide[1], Masahiro Nomura[1,2], Yukiko T. Matsunaga[1,2]*

The Starling principle describes exchanges between blood and tissues based on the balance of hydrostatic and osmotic flows. However, the permeation properties of the main constituent of tissues, namely, collagen, in response to the stress exerted by blood pressure remain poorly characterized. Here, we develop an instrument to determine the elasticity and permeability of collagen gels under tensile and compressive stress based on measuring the temporal change in pressure in an air cavity sealed at the outlet of a collagen slab. Data analysis with an analytical model reveals a drop in the permeability and enhanced strain stiffening of native collagen gels under compression versus tension, both effects being essentially lost after chemical cross-linking. Furthermore, we report the control of the permeability of native collagen gels using sinusoidal fluid injection, an effect explained by the asymmetric response in tension and compression. We lastly suggest that blood-associated pulsations could contribute to exchanges within tissues.

INTRODUCTION

Tissues constitute porous solid matrices traversed by fluid flows that convey oxygen and nutrients from the blood to cells and remove cellular waste products. Diseases and aging disrupt homeostasis by altering vascularization and remodeling tissue and, in turn, dysregulate diverse cellular functions, including proliferation, migration, and differentiation (*1*). The Starling principle describes fluid movements between blood and tissues as a balance between the hydrostatic and oncotic pressures (protein component of the osmotic pressure) (*2*, *3*). This model, which has recently been revised to include the effects of lymphatic systems enabling the fluid drainage in tissues (*4*), and its net balance are considered to be essential to enhance drug delivery (*5*). While hydrodynamic laws suffice to describe this process in rigid porous materials, the change of flows associated to mechanical deformation of soft liquid-filled matrices remains essentially overlooked in physiological transport models. The interaction between fluid flow and solid deformation is described by the poroelastic mechanics, which couples Darcy's law with Terzaghi's effective stress and linear elasticity (*6*–*8*). Poroelastic models predict that the filtration of liquid in a soft and porous tube differs from that of a stiff material through (i) the changes in the material permeability associated to its structure deformation and (ii) an additional solid flow. They rely on mechanical (elastic modulus) and hydraulic (permeability) parameters of poroelastic materials (*9*, *10*). To the best of our knowledge, however, poroelastic models have not yet been used to characterize the response and infer the physical properties of the main constituents of tissues, which are soft and permeable materials.

Collagen gels are extensively used as cell culture scaffolds, including organs-on-chip and organoids, due to their low immunogenicity and versatile elasticity associated to a shear modulus spanning 1 to 1000 Pa by tuning the gel concentration and reticulation temperature (*11*–*13*). They recapitulate the constant reorganization of tissues in vivo as a consequence of cellular traction forces (*14*, *15*). The permeability of these materials, which ensures the transport of solutes to promote cell growth and waste clearance, is also one of their assets (*16*). However, the permeability of collagen gels remains poorly estimated with data spanning two orders of magnitude from 10^{-14} to 10^{-12} m^2 in unstrained conditions (*17*–*19*). This discrepancy obtained with a similar collagen concentration may be resolved by considering that compressive stress can lower the permeability, but a decrease in permeability by two orders of magnitude implies a sizeable compressive stress (~700 Pa), raising questions on whether the coupling between mechanics and hydrodynamics has been accurately described in this material. This coupling should, however, not be overlooked because blood pressure is not only a driving force for interstitial fluid flows in tissues but also a source of mechanical stress that may contribute to modulate their permeation properties.

We reasoned that this imperfect description of collagen gel permeation properties was explained by the lack of methods to measure the permeability and elasticity of soft and porous hydrogels, which constitute a ubiquitous class of materials in tissue engineering (*20*). Hence, we developed a contact-free technology to characterize the poromechanic properties of reconstituted collagen networks under compressive and tensile stresses. Our method is based on a pressure sensor connected to an air cavity placed at the outlet of the material and a pressure controller to monitor the inlet. Therefore, this method relies on two sensors, whereas conventional techniques use pressure, flow, and deformation detection units (*21*). Supported by an analytical model to extract the permeability and elasticity of the gel and validated by finite element simulations, our instrument uncovers the asymmetry of the permeation and elastic properties of collagen gels for tensile and compressive stresses in the regime of reversible deformation, i.e., without permanent reorganization of

[1]Institute of Industrial Science, The University of Tokyo, Tokyo 153-8505, Japan. [2]LIMMS, CNRS-IIS IRL 2820, The University of Tokyo, Tokyo 153-8505, Japan. [3]LAAS-CNRS, Université de Toulouse, CNRS, Toulouse, France.
*Corresponding author. Email: abancaud@laas.fr (A.B.); mat@iis.u-tokyo.ac.jp (Y.T. M.)

the gel network as observed when applying the load with a mechanical piston (*22*–*24*). Last, by monitoring the response of this material to pulsatile pressure actuation, we find out that a periodic signal with zero mean value can generate a buildup in bulk compressive stress that, in turn, tunes the gel permeability.

RESULTS

Principle of the instrument

Our method is based on a pressure sensor connected to an air cavity placed at the outlet of a collagen slab (Fig. 1A and fig. S1). At the inlet, we apply tunable hydrostatic pressure loads, which induce solid and fluid displacements that compress the air in the cavity (Fig. 1B). Hence, it allows the deformation of the solid and the generation of a flow to contribute to the air cavity pressure response without directly measuring or imposing a flow rate and/or a mechanical constraint. Qualitatively, the response of the material to a step in pressure consists of an immediate solid deformation and a flux of liquid through the porous material (that is, a volume change that increases linearly with time). Hence, the elastic and hydrodynamic responses occur on separate time scales, enabling the permeability and elasticity of the material to be inferred from fitting the measured intracavity pressure to an analytical model described in the next section.

Poroelastic model of the pressure in the air cavity

Let us consider a homogeneous poroelastic material, in which the fluid and solid displacements are unidirectional between its inlet ($x = 0$) and outlet ($x = H$), as shown in Fig. 1A. According to Darcy's law, the permeation flow W is proportional to the pressure field $P(x, t)$ gradient, as follows

$$W = -\frac{\kappa}{\mu}\frac{\partial P}{\partial x} \tag{1}$$

where μ is the fluid viscosity and κ the material permeability. Given that the fluid and solid are incompressible and assuming the deformation to be small, linear poroelasticity models enable us to relate the pressure gradient in Eq. 1 to the displacement field $U(x, t)$ of the solid by the balance of mechanical equilibrium (*25*)

$$M\frac{\partial^2 U}{\partial x^2} = \frac{\partial P}{\partial x} \tag{2}$$

with M being the p-wave elastic modulus of the considered isotropic homogeneous material. Because the total flow rate of liquid and solid is conservative [$W + \partial U/\partial t = A(t)$, where $A(t)$ is a constant of integration], as defined by Kenyon (*7*), the combination of Eqs. 1 and 2 determines the spatial distribution and temporal evolution of the pressure and deformation fields. Notably, it is possible to use strain-dependent parameters for fibrous materials to model the permeability and elasticity. This approach enables the obtention of an explicit and integrated dependence on the porosity of the material (*9*, *10*), but the nonlinearity of the resulting model does not allow for an analytical solution. The boundary conditions consist of no displacement at the inlet and no contact stress at the outlet. The pressure is set to $P(0, t) = P_M$ starting from $t = 0$. The change in outlet pressure (i.e., in the air cavity) is dictated by the sum of the filtration velocity W and the solid velocity $\partial U/\partial t$. Assuming isothermal compression and defining V and P_A as the respective initial volume and pressure of the cavity, we obtain (see derivation in

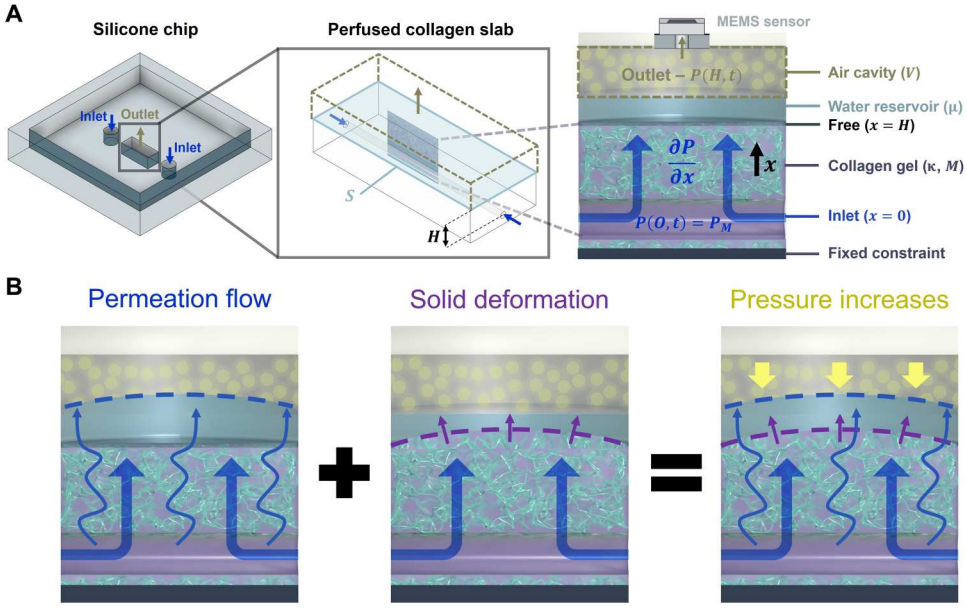

Fig. 1. Pressure sensing for poroelastic characterization. (**A**) Principle of the technology: A compartment filled with collagen gel is traversed by an inlet hollow tube of 200 μm in diameter, in which a pressure P_M is applied. On top, a MEMS -based (Microelectromechanical system) pressure sensor records the pressure variation in the air cavity $P(x = H, t)$. (**B**) A hydrostatic pressure load in the inlet induces a permeation flow and a solid deformation that increase the pressure in the cavity.

the Supplementary Materials)

$$\begin{cases} U(0,t) = 0 \\ \frac{\partial U}{\partial x}(H,t) = 0 \\ \frac{\partial P}{\partial t}(H,t) = \frac{SP_A}{V}\left[-\frac{\kappa}{\mu}\frac{\partial P}{\partial x}(H,t) + \frac{\partial U}{\partial t}(H,t)\right] \end{cases} \quad (3)$$

where $S = 15\ \text{mm}^2$ is the material cross section and $H = 0.8$ mm. The volume of the cavity V is set to 2 ml, so that relative changes in volume and pressure in the cavity are small, on the order of 10^{-3} (see details in the Supplementary Materials). The analytical solution of Eqs. 1 to 3 for the pressure kinetic response at the outlet position is (see details in the Supplementary Materials)

$$P(H,t) = P_M\left[1 - 2\sum_{n=1}^{\infty}\frac{\sin(2\lambda_n)e^{-\frac{\lambda_n^2 t}{\tau}}}{\sin(2\lambda_n) + 2\lambda_n}\right] \quad (4)$$

where $\tau = \mu H^2/\kappa M$ and λ_n are the roots of the relation $\alpha\lambda_n \tan(\lambda_n) = 1$ with $\lambda_n < \lambda_{n+1}$ and $\alpha = VM/SP_AH$. To explain the physical meaning of the variables τ and α, we suggest to consider the model situation of an open air cavity was opened [$P(H, t) = 0$]. At the steady state, we would have $U(H) = P_MH/2M$ and $W = \kappa P_M/\mu H$. The characteristic time $\tau = 2U(H)/W$ then represents the ratio between twice the displacement and the filtration velocity, while α is the ratio of the inlet pressure to the pressure change induced by the solid deformation. Note lastly that the bending of the collagen along the direction of the tube is neglected in our one-dimensional (1D) model, as the length of the collagen slab is much larger than its height.

For a relatively stiff porous material (i.e., $M \gg P_ASH/V$), the contribution of the solid deformation to the cavity pressurization can be neglected, the parameter α becomes much greater than unity ($\alpha \gg 1$), and, therefore, $\lambda_n \approx 1/\sqrt{\alpha}$ and $\sin(2\lambda_n) \approx 2\lambda_n$. After inserting these results into Eq. 4, the following mono-exponential relaxation for the intracavity pressure is obtained

$$P(H,t) = P_M(1 - e^{-\frac{t}{\alpha\tau}}) \quad (5)$$

Equation 5 can also be obtained by neglecting the deformation of the solid in Eq. 3 and assuming a linear pressure gradient. This mono-exponential regime can readily be tested using an isoporous polycarbonate membrane (IT4IP) with homogeneous pores of radius $r_p = 0.9$ μm and density $\rho = 3.6 \times 10^5\ \text{cm}^{-2}$. According to these specifications, the permeability of this membrane is given by $\rho\pi r_p^4/8$ and is, therefore, equal to $9.3 \times 10^{-16}\ \text{m}^2$. Considering that the elastic modulus of polycarbonate is ~2 GPa (*26*) and the height of the membrane is ~50 μm, we conclude that $\alpha \sim 10^8$, for a cavity of volume $V = 2$ ml. Hence, the cavity pressurization is well determined by the permeation, and the pressure kinetic data accordingly follow an exponential relaxation (fig. S2). The fit with Eq. 5 yields a permeability of $(8.7 \pm 1.1) \times 10^{-16}\ \text{m}^2$, which is in excellent agreement with the value inferred from the product datasheet.

Next, we investigate the model predictions for soft poroelastic materials. The evolution of pressure $P(H, t)$ with time is shown in Fig. 2A, for a representative set of permeabilities (10^{-13} to $10^{-15}\ \text{m}^2$) and elastic moduli (500 to 4000 Pa). In contrast to the exponential relaxation of rigid porous materials (black solid curves), the deformation of the solid speeds up the compression of the cavity in the short-time limit, such that the softer the material, the faster the initial pressure increase. Conversely, the typical relaxation rate in the long-time limit is readily dictated by the permeability, as shown by the clear separation of the relaxation curves for 10^{-13}, 10^{-14}, and $10^{-15}\ \text{m}^2$. The highest sensitivity of the pressure model to M and κ, therefore, appears at different time scales, as confirmed by the sensitivity analysis developed in the Supplementary Materials (fig. S3). This fact indicates that both parameters, M and κ, can accurately be retrieved from relaxation data.

Last, we aimed to validate the relevance of the 1D model for our experimental setup, in which the inlet pressure is actually injected through a tube, as described in Fig. 1A. We performed finite element simulations with the 2D section geometry of the collagen slab using COMSOL (Fig. 2B and Materials and Methods). The comparison of the simulations and the 1D model (Fig. 2C) for the same set of poroelastic parameters ($M \in [500, 4000]$ Pa and $\kappa \in [10^{-15}, 10^{-13}]\ \text{m}^2$) showed an excellent agreement. This agreement was obtained by defining a correction parameter γ, as defined by $\kappa_c = \kappa/\gamma$ and $M_c = \gamma M$ with the index c standing for COMSOL variables. This correction factor, which corresponded to a geometrical correction to match the 1D model with the fluid injection through a tube in real settings, was equal to 1.77 for all the simulations. Note that this correction factor is dependent on the geometrical settings of the collagen gel.

Poroelastic characterization of collagen gels

We prepared collagen gels at a concentration of 2.4 mg/ml using thermal gelation at 37°C during 45 min using the protocol described in (*27*). Collagen gels were either used in their native conformation (non-cross-linked) or cross-linked (CL) with paraformaldehyde at a concentration of 4% for 10 hours (*28*). The pressure response in the cavity was recorded for actuation pressures in the range of 100 to 1000 Pa (red and blue datasets with positive values in Fig. 3, A and B). In these settings, collagen properties are probed in tension because the material bulges and expands in the cavity due hydrostatic stress (top inset in Fig. 3A). The kinetics of pressure relaxation took about 60 s, and, after this transient phase, the pressure was the same in the inlet and in the air cavity. We then released the pressure at the inlet and recorded the decrease of intracavity pressure. In the second step of the experiment, collagen is in compression because the pressure in the cavity is greater than that in the inlet (bottom inset in Fig. 3A, and curves in the light gray sectors of Fig. 3, A and B). We note that these experiments could be reproduced at least three times consecutively with the same kinetic response in the cavity. Our data indicate a marked slowdown of the relaxation dynamics in compression for native versus CL collagen gels, whereas the responses in tension are comparable. While presented experiments were conducted with pepsin solubilized collagen, this response was detected independently of the collagen purification method, including acid soluble collagen (fig. S4). For every experimental condition, the 1D model and 2D COMSOL simulations enabled us to obtain excellent fits (Fig. 3, C and D) and to infer the effective values of M and κ. Notably, as the gel is clamped at the inlet and free at the outlet, its deformation is nonuniform, and the relevance of the hypothesis of linear elastic properties can be questioned. The assumption of small deformations, as validated by the quality of the fits, is justified by the strong mechanical constraints exerted by the grafting of collagen to the bottom glass surface used in our experimental setup. This hypothesis could, nevertheless, be leveraged by integrating nonlinear parameters for the elasticity and permeability using, e.g., the J2 deformation theory of

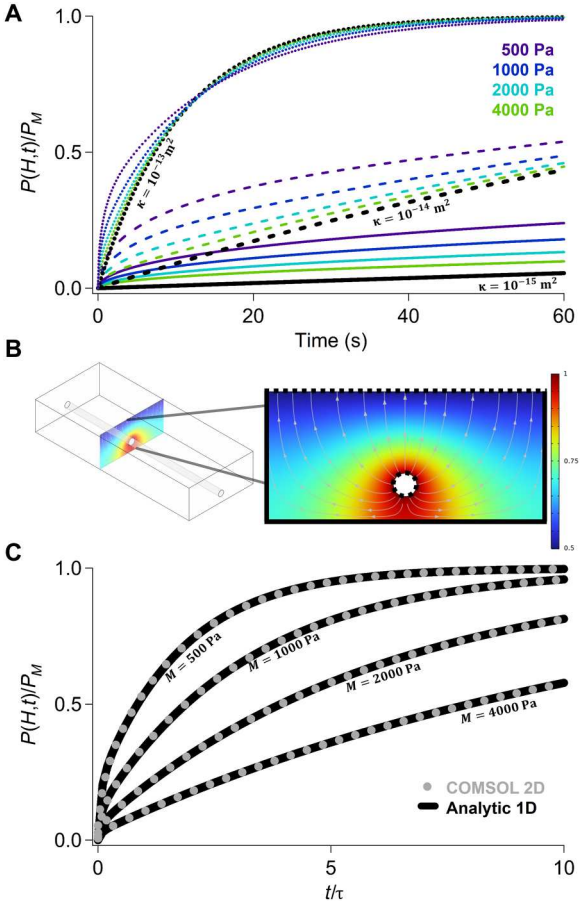

Fig. 2. Predictions of the 1D model and validation by finite element simulations. (**A**) Intracavity pressure kinetic response predicted by the one-dimensional (1D) model for a p-wave modulus $M \in [500, 4000]$ Pa and three representative values (10^{-13}, 10^{-14}, and 10^{-15} m^2) of the permeability κ. The three black curves correspond to the limit of a rigid porous material described by Eq. 5. (**B**) The scheme on the left is the configuration of the collagen slab for finite element simulations. The collagen is clamped on its sides and at the bottom (black solid lines), and the injection tube and top interface are free (dashed lines). The colormap shows the simulated normalized pressure field. (**C**) The plot shows the comparison of the 1D kinetic model for the same parameters as in (A) and the numerical simulations (solid curves and dotted datasets, respectively). Note that the time was normalized by τ to collapse the curves of the model presented in (A).

plasticity for fibrous systems (*29*) and the Kozeny-Carman model of permeability (*30*), respectively.

The fits explained the slow kinetics in native collagen networks by the reduced permeability in compression by a factor of 4 (Fig. 3D). This asymmetric response of native collagen gel in compression versus tension, which is reminiscent of the exponential reduction of cartilage permeability under compression (*31*), became roughly symmetrical after CL. Similarly, the strain-stiffening response of the network, an effect thoroughly described in the literature (*11*), was strongly and mildly asymmetrical in tension versus compression for native and CL collagen, respectively (Fig. 3C). Notably, the tensile elastic modulus increased linearly with the applied stress, in agreement with the data of (*11*–*13*), and its amplitude was typically two times larger for CL collagen gels. Conversely, the compressive elastic modulus of native collagen became stiffer than that of CL collagen at high load, whereas it was softer below 200 Pa. Together, native collagen gel is characterized by strain-dependent permeability and asymmetrical strain stiffening in tension and compression, both effects being reduced or removed by chemical CL.

To investigate the origin of these asymmetric properties, we characterized the microstructure of collagen networks by immunofluorescence confocal microscopy focusing right on top of the pressure inlet. The structure showed that the fixation process induced the collapse of the dense native network onto a "primitive" backbone with an increase in pore size. The loose meshwork of CL collagen gels remained stable under tensile and compressive stresses of 100 Pa (fig. S5). This observation was consistent with the steady value of the permeability of this material under tension and compression. Contrariwise, the microstructure of native collagen gels markedly changed in compression versus tension (Fig. 3E). After binarization, the images were analyzed to extract the pore size, as described in the Supplementary Materials (fig. S5B). We then plotted the cumulative density function of the gel pore radius (Fig. 3F). This cumulative density function was fitted with a Gaussian model to infer the mean pore radius for native collagen under tension and compression of 1.52 and 1.19 μm, respectively. This variation in pore size was not detected in CL collagen (fig. S5C). We suggest that the denser meshwork in compression is associated to enhance hydrodynamic interactions within the pores and accounts for the strain-dependent permeability. We conclude that microstructural analysis supports the asymmetrical permeability of collagen gels detected by pressure measurements.

Periodic pressure actuation

Capillary blood pressure consists of a continuous component of ~2000 Pa and periodic pulses, which are characterized by a typical frequency ω_0 of 1 Hz and a magnitude of 100 to 1000 Pa (*32*). We investigated the consequences of this periodic component using a sinusoidal input pressure P_M of amplitude 200, 400, and 800 Pa. After a transient of a few cycles, a permanent regime of oscillations was reached in the cavity, allowing us to compute the pressure averaged over 100 cycles (Fig. 4, A and B). Note that we did not detect any drift during the periodic actuation phase. The amplitude of the signal in the cavity was ~4% of the input, equivalently ~10 Pa. Using CL collagen gels, the pressure in the cavity had symmetric positive and negative half-cycles and was centered at $P_M/2$, and its amplitude was proportional to P_M (Fig. 4B). By contrast, native collagen network response markedly changed as the pressure increased. For 200 Pa, the signal was symmetrical and centered at $P_M/2$, but positive and negative half-cycles became increasingly asymmetrical as the pressure increased from 400 to 800 Pa (Fig. 4A). This response was associated to an increase of the mean pressure in the cavity to $0.67 \times P_M$ at 800 Pa (inset of Fig. 4A). Hence, periodic pressure was associated to an accumulation of compressive stress in native, but not CL, collagen gels at the steady state, and set this material in the regime of sharp variation of its permeability (Fig. 3D).

The accumulation of compressive stress can readily be understood from the elegant analysis of pressure consolidation in poroelastic materials proposed by Kenyon (*33*). Fluid injection with a step in pressure is associated to a diffusion-like propagation of the pressure field in the material (*25*). The effective diffusion coefficient D scales as $\kappa M/\mu$, resulting in a consolidation layer of comparable

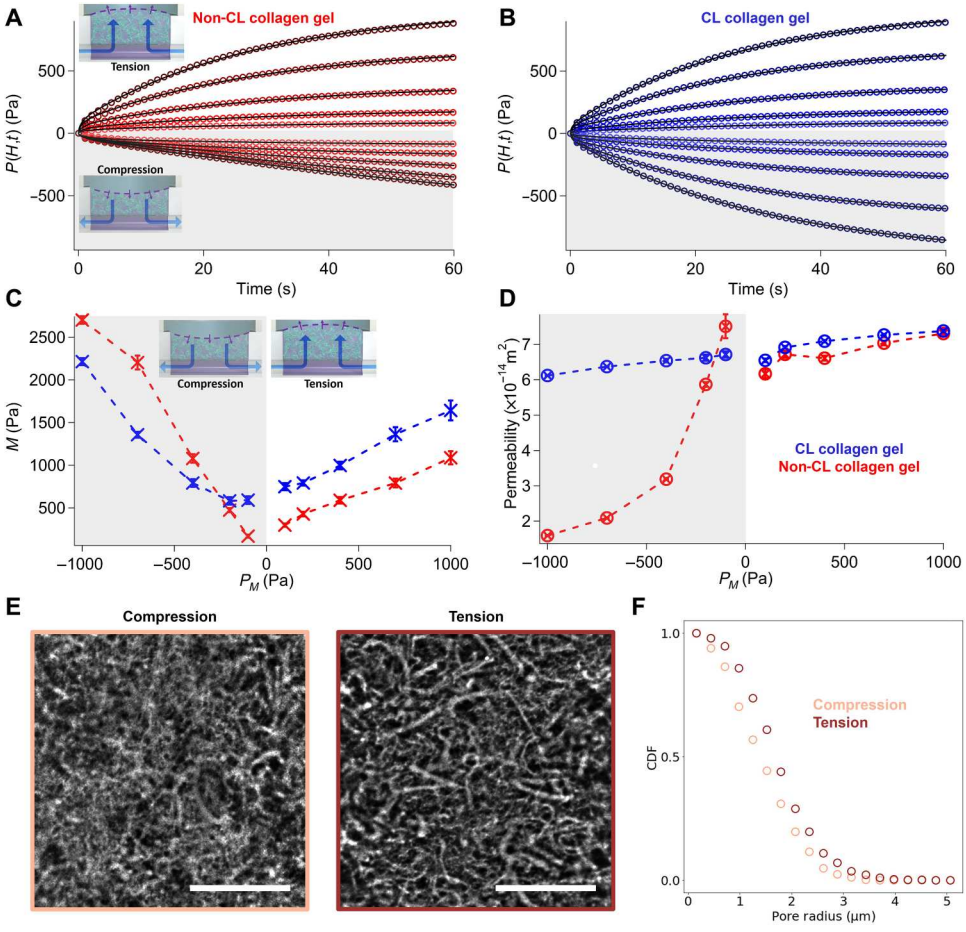

Fig. 3. Poroelastic analysis of type I collagen gel. (**A**) Before and (**B**) after chemical CL for a pressure P_M ranging from 100 to 1000 Pa. The fitted parameters M and κ are plotted as functions of the actuation pressure P_M in (**C**) and (**D**), respectively. The dataset for native and CL collagen are reported in red and blue, respectively. (**E**) Representative confocal micrographs of native (in red) collagen microstructure under compression (−100 Pa) and under tension (+100 Pa). The confocal micrograph thickness is 2 μm, as obtained with a 40× water immersion objective. The scale bars correspond to 40 μm. (**F**) Cumulative density function (CDF) of the pore radius in non-CL collagen after image analysis giving a pore radius of 1.19 μm in compression and 1.52 μm in tension.

thickness in tension and in compression of $\sqrt{D \times \pi/\omega_0}$ ~140 μm. Liquid is, hence, soaked into and expelled from the collagen gel during the cycles of tension and compression, respectively. The flow velocity during each cycle is typically determined by the pressure gradient in the consolidation layer and the permeability

$$W \sim \frac{\kappa}{\mu}\frac{P_M}{\sqrt{D \times \pi/\omega_0}} = \sqrt{\frac{\kappa}{\mu M}}\frac{P_M}{\sqrt{\pi/\omega_0}} \quad (6)$$

The asymmetric response of collagen is characterized by a reduced permeability and an increased elasticity in compression by the same typical factor of 4. Hence, the velocity W is reduced by a factor of 4 in compression versus tension. Mass conservation implies that the same amount of fluid is expelled and soaked during compressive and tensile cycles. This condition is fulfilled if the soaking phase is shorter than that of expulsion, as insured by the offset in bulk compressive stress. We note that this offset in compressive stress enables the dynamic modulation of collagen gel permeation properties. This is shown by monitoring the kinetic response to a step of pressure of 500 Pa with a permanent periodic pulsatile flow associated to an amplitude 100, 200, and 400 Pa (dark, plain, and light red curves in Fig. 4C). The relaxation became slower as the amplitude of the periodic stimulation increased, in agreement with the fact that periodic forcing set collagen in conditions of low permeability. The fit of the curves with the model of Eq. 4 (dashed black curves in Fig. 4C) confirmed our hypothesis because the permeability was 35% lower for high-amplitude pulsations and the elastic modulus was unchanged (inset of Fig. 4C).

DISCUSSION

We have developed a methodology and its analytical model for the characterization of virtually any poroelastic material. Applied to type I collagen gels, the method allows us to show that this material is characterized by enhanced strain stiffening and reduced permeability in compression. These two properties, which have been uncovered with a 1D linear model, are still to be investigated with sophisticated nonlinear models and connected to the well-described mechanism of collagen matrix densification (*34*, *35*). Nevertheless, we suggest that they may have profound consequences on the transport in biological tissues in the context of the extended Starling

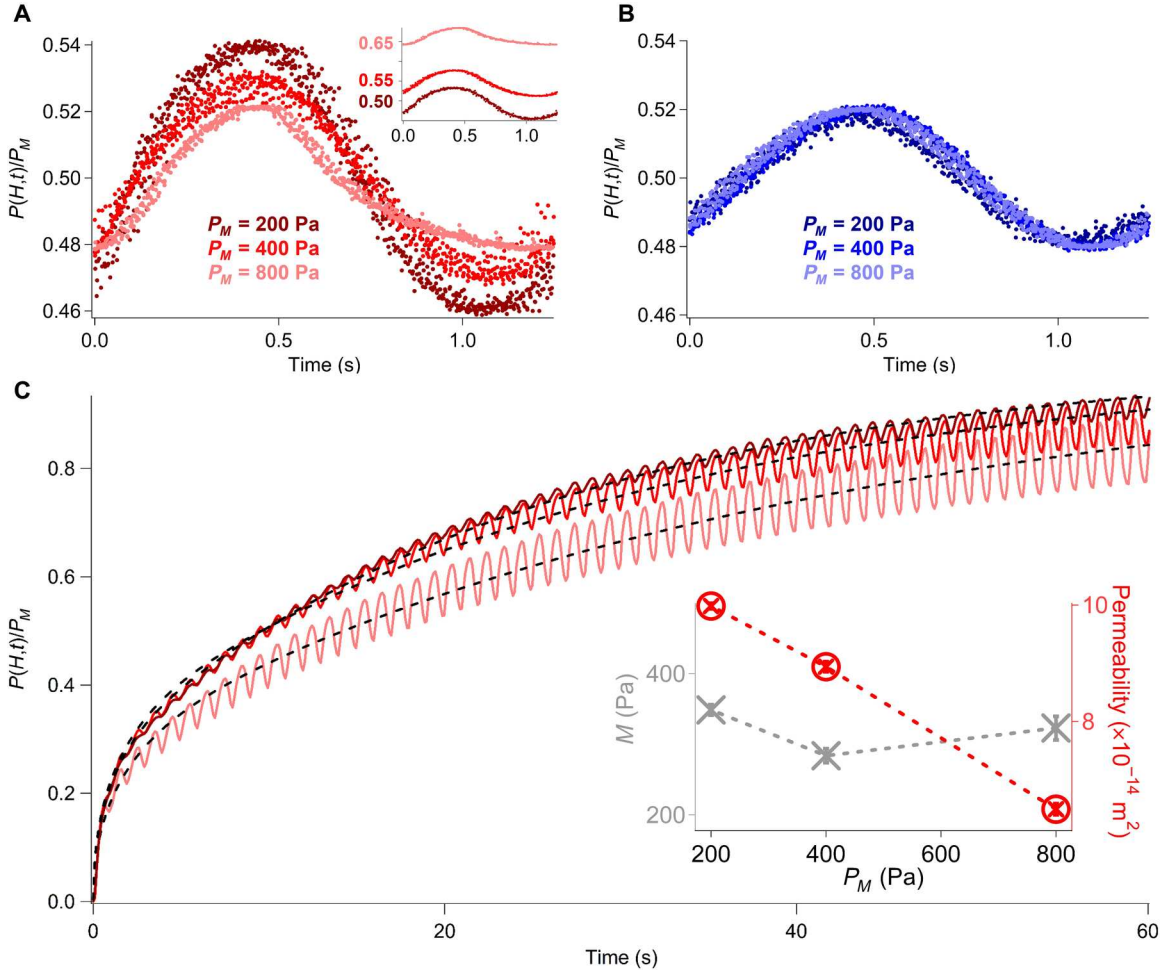

Fig. 4. Collagen gel response to periodic actuation. (**A**) The intracavity pressure averaged over 100 cycles for native collagen is normalized and registered at 0.5 for different pressure settings. The inset shows the same raw datasets without registration at 0.5. (**B**) The same experiment is carried out with CL collagen, and the three recordings are only normalized to the input pressure. (**C**) The response of collagen to a step-in pressure is dependent on the magnitude of the amplitude of periodic pressure actuation. The recordings in dark red, red, and light red correspond to an actuation pressure of 200, 400, and 800 Pa, respectively. The dashed lines are the fits with the model in Eq. 4, and fitted parameters, *M* and κ, are plotted in the inset.

principle (*3*). Considering the "healthy" situation of a steady interstitial flow between blood and lymphatic microvessels, pulsatile intraluminal pressure in the blood circulation network creates a compressive stress that tends to reduce permeation flux. Lymphatic drainage vanishes this stress, likely facilitating a clearance in the tissue by enhancing the permeability (*36*). Upon physical efforts, the increase of blood pressure is associated to high-amplitude pulsatile flows that are likely to reduce the permeability of the tissue, hence hinting at a passive regulatory role of native extracellular matrices to control homeostasis. If we now consider the pathological environment of tumors, then we suggest that the mechanical compression induced by the tumor mass cannot be reset by the lymphatic system, reducing drainage and enhancing hypoxia (*37*). This effect may be further enhanced by tissue remodeling in the tumor environment (*38*), because the enriched concentration of collagen is expected to lower the tissue permeability. Consequently, poroelastic properties of tissues and their alteration during tissue remodeling by, e.g., tumor growth appear as an underestimated player of homeostatic regulation and drug transport mechanisms, which could be studied and quantified with microphysiological systems. In this sense and to get closer to the physiological tissue properties, we are now characterizing hydrogels seeded with different cell types (e.g., fibroblasts and astrocytes) that reshape the collagen gel structure and change its composition.

MATERIALS AND METHODS

Collagen gel chips were fabricated using the microvessel chips described in (*27*). The silicone chips and 200-μm acupuncture needles(no. 08, J type; Seirin, Shizuoka, Japan) were first placed together in a vacuum reactor with 100 μl of aminopropyl-triethoxysilane and left at 0.1 mbar and room temperature for 30 min. Needles were then soaked in 1% (m:v) bovine serum albumin, dried, and sterilized by ultraviolet light exposure. The chips were treated with 50 μl of 2.5% glutaraldehyde for 1 min, then thoroughly rinsed with water, and dried. The collagen solution was subsequently prepared on ice by mixing Cellmatrix Type I-P (pepsin solubilized) solution (Nitta Gelatin, Japan), 10× Hanks′ buffer, and 10× collagen buffer

(volume ratio, 8:1:1) following the manufacturer's protocol. For comparison, we also used Cellmatric Type I-A (acid soluble collagen) solution from the same supplier, as presented in the SM.We poured 30 μl of this ice-cold collagen solution into the chip, inserted the coated needle, and incubated the system at 37°C for 40 min to allow collagen reticulation. The needle was withdrawn to form a hollow channel, and the chips were left in a phosphate buffer. Note that this protocol chemically clamps the collagen gel to the glass and silicone surfaces (see Fig. 1A).

The collagen gel embedded within a silicone chip was connected to a pressure controller (Fluigent MFCS) and a pressure sensor (Merit Sensor LP series) by mean of 3D printed mechanical pieces (Elegoo Mars 3, water washable resin). Acquisition was done through a dedicated LabVIEW interface allowing the control of the inlet pressure while recording the outlet signal with a digital multimeter (Agilent, 34401A). The resulting data were fitted by coding the analytical solution (Eq. 4) in MATLAB and using the "fit" function to retrieve M and κ.

Simulations were run with COMSOL Multiphysics 6.0 using the linear poroelastic module, which allowed coupling of the Darcy's law and the solid mechanics modules. We set the tube radius r_0 to 100 μm and placed it 300 μm above the glass coverslip and 0.8 mm from the top outlet of collagen. The collagen slab was 2.5 mm in width and 1.1 mm in height. An inlet pressure P_M was imposed onto the collagen gel channel border, creating a double boundary condition defined as a pressure in the Darcy's law module and a boundary load in the solid mechanics module. We used the "boundary ODEs (ordinary differential equations) and DAEs (differential-algebraic equations)" module to solve the boundary condition in the air cavity.

Immunofluorescence confocal microscopy was performed with the LSM 700 confocal microscope (Carl Zeiss) equipped with a 40× water immersion objective (numerical aperture of 1.2) and using a pinhole of 1 Airy unit. The microstructure of native or cross-linked collagen gells was observed after incubation with the conjugate of mouse monoclonal anti-collagen I antibody (ab6308, Abcam, Cambridge, UK) and Alexa Fluor 488-labeled donkey antibody agonist mouse IgG diluted at 1:100 in blocking solution for 4 hours, and then rinsing the gel with phosphate buffer The chip was mounted on the pressure sensing system, opening the pressure sensor outlet to apply a steady pressure gradient over time. Images were eventually analyzed with PoreSpy (*39*) in Python using a drainage algorithm for porosimetry.

Supplementary Materials

This PDF file includes:

Figs. S1 to S5
Definition of the boundary condition in the cavity
1D model: Laplace transform

REFERENCES AND NOTES

1. C. Bonnans, J. Chou, Z. Werb, Remodelling the extracellular matrix in development and disease. *Nat. Rev. Mol. Cell Biol.* **15**, 786–801 (2014).
2. E. H. Starling, On the absorption of fluids from the connective tissue spaces. *J. Physiol.* **19**, 312–326 (1896).
3. C. C. Michel, T. E. Woodcock, F.-R. E. Curry, Understanding and extending the Starling principle. *Acta Anaesthesiol. Scand.* **64**, 1032–1037 (2020).
4. T. E. Woodcock, T. M. Woodcock, Revised Starling equation and the glycocalyx model of transvascular fluid exchange: An improved paradigm for prescribing intravenous fluid therapy. *Br. J. Anaesth.* **108**, 384–394 (2012).
5. C. A. Stine, J. M. Munson, Convection-enhanced delivery: Connection to and impact of interstitial fluid flow. *Front. Oncol.* **9**, 966 (2019).
6. M. A. Biot, General theory of three-dimensional consolidation. *J. Appl. Phys.* **12**, 155–164 (1941).
7. D. E. Kenyon, Transient filtration in a porous elastic cylinder. *J. Appl. Mech.* **43**, 594–598 (1976).
8. G. Jayaraman, Water transport in the arterial wall—A theoretical study. *J. Biomech.* **16**, 833–840 (1983).
9. L. C. Auton, C. W. MacMinn, From arteries to boreholes: Steady-state response of a poroelastic cylinder to fluid injection. *Proc. Math. Phys. Eng. Sci.* **473**, 20160753 (2017).
10. L. C. Auton, C. W. MacMinn, From arteries to boreholes: Transient response of a poroelastic cylinder to fluid injection. *Proc. Math. Phys. Eng. Sci.* **474**, 20180284 (2018).
11. A. J. Licup, S. Münster, A. Sharma, M. Sheinman, L. M. Jawerth, B. Fabry, D. A. Weitz, F. C. MacKintosh, Stress controls the mechanics of collagen networks. *Proc. Natl. Acad. Sci. U.S.A.* **112**, 9573–9578 (2015).
12. S. Nam, K. H. Hu, M. J. Butte, O. Chaudhuri, Strain-enhanced stress relaxation impacts nonlinear elasticity in collagen gels. *Proc. Natl. Acad. Sci. U.S.A.* **113**, 5492–5497 (2016).
13. E. Ban, H. Wang, J. M. Franklin, J. T. Liphardt, P. A. Janmey, V. B. Shenoy, Strong triaxial coupling and anomalous Poisson effect in collagen networks. *Proc. Natl. Acad. Sci. U.S.A.* **116**, 6790–6799 (2019).
14. E. Ban, J. M. Franklin, S. Nam, L. R. Smith, H. Wang, R. G. Wells, O. Chaudhuri, J. T. Liphardt, V. B. Shenoy, Mechanisms of plastic deformation in collagen networks induced by cellular forces. *Biophys. J.* **114**, 450–461 (2018).
15. J. Kim, J. Feng, C. A. R. Jones, X. Mao, L. M. Sander, H. Levine, B. Sun, Stress-induced plasticity of dynamic collagen networks. *Nat. Commun.* **8**, 842 (2017).
16. C. Dong, Y. Lv, Application of collagen scaffold in tissue engineering: Recent advances and new perspectives. *Polymers* **8**, 42 (2016).
17. E. Gentleman, E. A. Nauman, K. C. Dee, G. A. Livesay, Short collagen fibers provide control of contraction and permeability in fibroblast-seeded collagen gels. *Tissue Eng.* **10**, 421–427 (2004).
18. V. Serpooshan, M. Julien, O. Nguyen, H. Wang, A. Li, N. Muja, J. E. Henderson, S. N. Nazhat, Reduced hydraulic permeability of three-dimensional collagen scaffolds attenuates gel contraction and promotes the growth and differentiation of mesenchymal stem cells. *Acta Biomater.* **6**, 3978–3987 (2010).
19. V. Serpooshan, T. M. Quinn, N. Muja, S. N. Nazhat, Hydraulic permeability of multilayered collagen gel scaffolds under plastic compression-induced unidirectional fluid flow. *Acta Biomater.* **9**, 4673–4680 (2013).
20. Y. S. Zhang, A. Khademhosseini, Advances in engineering hydrogels. *Science* **356**, eaaf3627 (2017).
21. C. S. Vidmar, M. Bazzi, V. K. Lai, Computational and experimental comparison on the effects of flow-induced compression on the permeability of collagen gels. *J. Mech. Behav. Biomed. Mater.* **128**, 105107 (2022).
22. P. Andrikakou, K. Vickraman, H. Arora, On the behaviour of lung tissue under tension and compression. *Sci. Rep.* **6**, 36642 (2016).
23. A. D. Drozdov, J. de Clavilee Christiansen, Tension–compression asymmetry in the mechanical response of hydrogels. *J. Mech. Behav. Biomed. Mater.* **110**, 103851 (2020).
24. M. Böl, S. Kohn, K. Leichsenring, E. Morales-Orcajo, A. E. Ehret, On multiscale tension-compression asymmetry in skeletal muscle. *Acta Biomater.* **144**, 210–220 (2022).
25. A. Malandrino, E. Moeendarbary, poroelasticity of living tissues, in *Encyclopedia of Biomedical Engineering* (Elsevier, 2019), pp. 238–245; https://linkinghub.elsevier.com/retrieve/pii/B978012801238399932X.
26. T. Pasman, D. Grijpma, D. Stamatialis, A. Poot, Flat and microstructured polymeric membranes in organs-on-chips. *J. R. Soc. Interface* **15**, 20180351 (2018).
27. J. Pauty, R. Usuba, I. G. Cheng, L. Hespel, H. Takahashi, K. Kato, M. Kobayashi, H. Nakajima, E. Lee, F. Yger, F. Soncin, Y. T. Matsunaga, A vascular endothelial growth factor-dependent sprouting angiogenesis assay based on an in vitro human blood vessel model for the study of anti-angiogenic drugs. *EBioMedicine* **27**, 225–236 (2018).
28. L. H. H. Olde Damink, P. J. Dijkstra, M. J. A. Van Luyn, P. B. Van Wachem, P. Nieuwenhuis, J. Feijen, Glutaraldehyde as a crosslinking agent for collagen-based biomaterials. *J. Mater. Sci. Mater. Med.* **6**, 460–472 (1995).
29. J. W. Hutchinson, K. W. Neale, Finite strain J2 deformation theory, in *Proceedings of the IUTAM Symposium on Finite Elasticity*, D. E. Carlson, R. T. Shield, Eds. (Springer Netherlands, Dordrecht, 1982), pp. 237–247.
30. P. C. Carman, Fluid flow through granular beds. *Chem. Eng. Res. Des.* **75**, S32–S48 (1997).
31. V. C. Mow, M. H. Holmes, W. M. Lai, Fluid transport and mechanical properties of articular cartilage: A review. *J. Biomech.* **17**, 377–394 (1984).

32. M. Hahn, T. Heubach, A. Steins, M. Jünger, Hemodynamics in nailfold capillaries of patients with systemic scleroderma: Synchronous measurements of capillary blood pressure and red blood cell velocity. *J. Invest. Dermatol.* **110**, 982–985 (1998).
33. D. Kenyon, A mathematical model of water flux through aortic tissue. *Bull. Math. Biol.* **41**, 79–90 (1979).
34. J. Ferruzzi, M. Sun, A. Gkousioudi, A. Pilvar, D. Roblyer, Y. Zhang, M. H. Zaman, Compressive remodeling alters fluid transport properties of collagen networks – Implications for tumor growth. *Sci. Rep.* **9**, 17151 (2019).
35. T. Novak, B. Seelbinder, C. M. Twitchell, C. C. van Donkelaar, S. L. Voytik-Harbin, C. P. Neu, Mechanisms and microenvironment investigation of cellularized high density gradient collagen matrices via densification. *Adv. Funct. Mater.* **26**, 2617–2628 (2016).
36. J. P. Scallan, S. D. Zawieja, J. A. Castorena-Gonzalez, M. J. Davis, Lymphatic pumping: Mechanics, mechanisms and malfunction. *J. Physiol.* **594**, 5749–5768 (2016).
37. E. Henke, R. Nandigama, S. Ergün, Extracellular matrix in the tumor microenvironment and its impact on cancer therapy. *Front. Mol. Biosci.* **6**, 160 (2019).
38. J. M. Munson, A. C. Shieh, Interstitial fluid flow in cancer: Implications for disease progression and treatment. *Cancer Manag Res.* **6**, 317–328 (2014).
39. J. T. Gostick, Z. A. Khan, T. G. Tranter, M. D. R. Kok, M. Agnaou, M. Sadeghi, R. Jervis, PoreSpy: A python toolkit for quantitative analysis of porous media images. *J. Open Source Softw.* **4**, 1296 (2019).

Acknowledgments: We thank T. Ando for artwork and R. Tan for English proofreading. We also thank P. Assemat for help in setting up the COMSOL simulations. **Funding:** J.C. acknowledges the JSPS for a postdoctoral fellowship. D.A. acknowledges the WINGS-QSTEP program for doctoral fellowship. We thank the LIMMS (CNRS–Institute of Industrial Science, University of Tokyo) for financial support. This research was partly supported by the Grant-in-Aid for JSPS Fellows (20F20806), AMED P-CREATE (JP18cm0106239h0001), and JSPS Core-to-Core Program (JPJSCCA-20190006). **Author contributions:** Conceptualization: J.C., A.B., and J.O.-M. Formal analysis: J.C. and D.A. Methodology: J.C., A.B., and J.O.-M. Investigation: J.C. Software: L.J. Visualization: J.C. and D.A. Funding acquisition: Y.T.M. and J.C. Supervision: J.C., A.B., and Y.T.M. Writing—original draft: J.C. and A.B. Writing—review and editing: J.C., A.B., J.O.-M., Y.T.M., M.N., and L.J. **Competing interests:** J.C., A.B., L.J., and Y.T.M. have a filed patent associated to the technology presented in the article (PCT no. EP2023053024; date: 7 February 2023). The other authors declare that they have no competing interests. **Data and materials availability:** All data needed to evaluate the conclusions in the paper are present in the paper and/or the Supplementary Materials.

Submitted 1 December 2022
Accepted 29 June 2023
Published 2 August 2023
10.1126/sciadv.adf9775

ScienceAdvances

Asymmetry of tensile versus compressive elasticity and permeability contributes to the regulation of exchanges in collagen gels

Jean Cacheux, Jose Ordonez-Miranda, Aurlien Bancaud, Laurent Jalabert, Daniel Alcaide, Masahiro Nomura, and Yukiko T. Matsunaga

Sci. Adv., **9** (31), eadf9775.
DOI: 10.1126/sciadv.adf9775

Science Advances (ISSN) is published by the American Association for the Advancement of Science. 1200 New York Avenue NW, Washington, DC 20005. The title *Science Advances* is a registered trademark of AAAS.